Electronic Supplementary Information (ESI)

For

Facile Electroless Displacement Plating of Mesoporous Gold Films as Robust and Reproducible SERS Substrates for Biosensing

Daiki Masaoka,[#a] Kaito Kono,[#a] Mostafa Kamal Masud,[b] Carlos Salomon,[c] Md Shahriar A. Hossain,[d] Asep Sugih Nugraha,[b] Joel Henzie,[e] Yusuke Asakura,[a] Emtiaz Ahmed,*[b] Mandy Hei Man Leung,*[a,f] Yusuke Yamauchi*[a,b]

[a]Department of Materials Process Engineering, Graduate School of Engineering, Nagoya University, Nagoya, Aichi, 464-8603, Japan.

[b]Australian Institute for Bioengineering and Nanotechnology (AIBN), The University of Queensland, Brisbane, QLD-4072, Australia.

[c]Centre for Clinical Diagnostics, University of Queensland Centre for Clinical Research, Brisbane, QLD-4029, Australia.

[d]School of Mechanical and Mining Engineering, The University of Queensland, Brisbane, QLD-4072, Australia.

[e]Research Center for Materials Nanoarchitectonics (MANA), National Institute for Materials Science (NIMS), Tsukuba, Ibaraki 305-0044, Japan

[f]Institute for Advanced Research (IAR), Nagoya University, Nagoya, Aichi, 464-8601, Japan.

# Equal contributions

*Corresponding authors emails: y.yamauchi@uq.edu.au; e.ahmed@uq.edu.au; leung.hei.man.f2@f.mail.nagoya-u.ac.jp

Supplementary Figures:

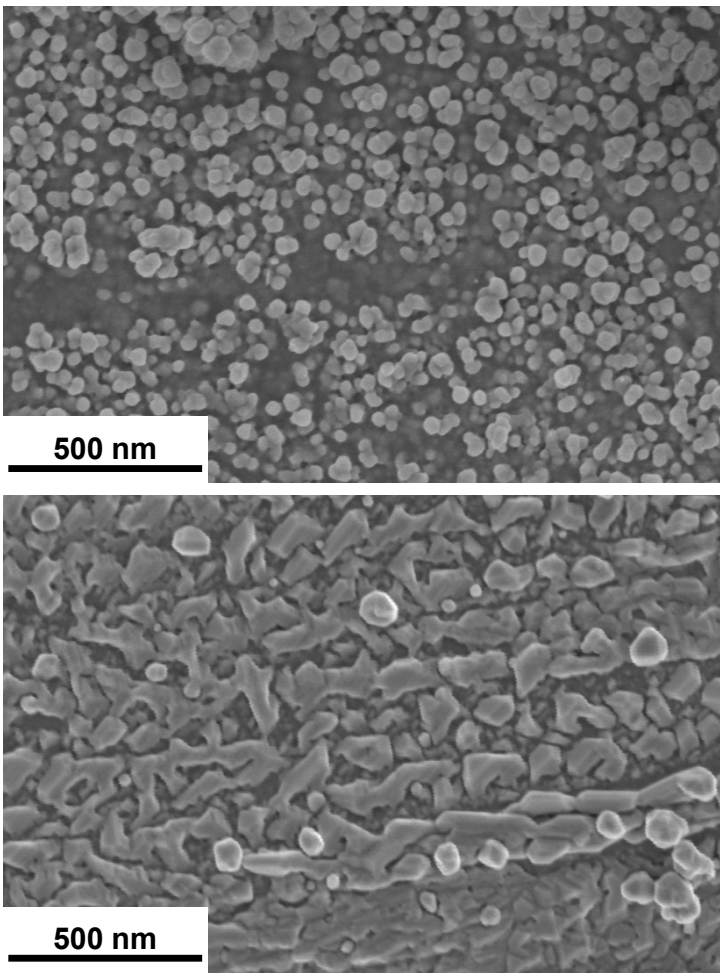

Fig. S1: SEM images of non-porous Au (top) and Ag (bottom) film on Cu substrate obtained in the absent of block polymer.

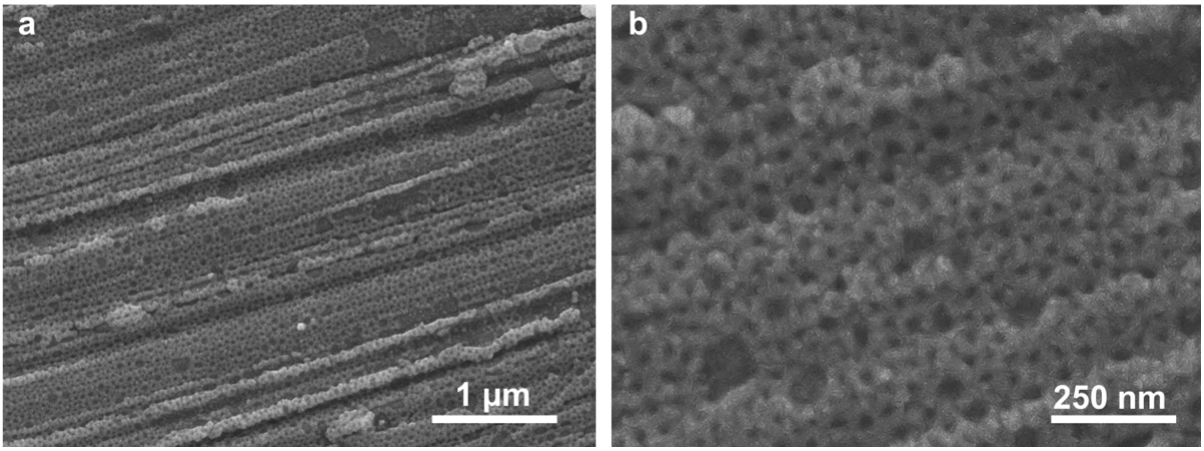

Fig. S2: SEM images of the mesoporous Au film prepared by micelle-assisted electroless chemical deposition on gold-coated silicon wafer: (a) low-magnification and (b) high-magnification views.

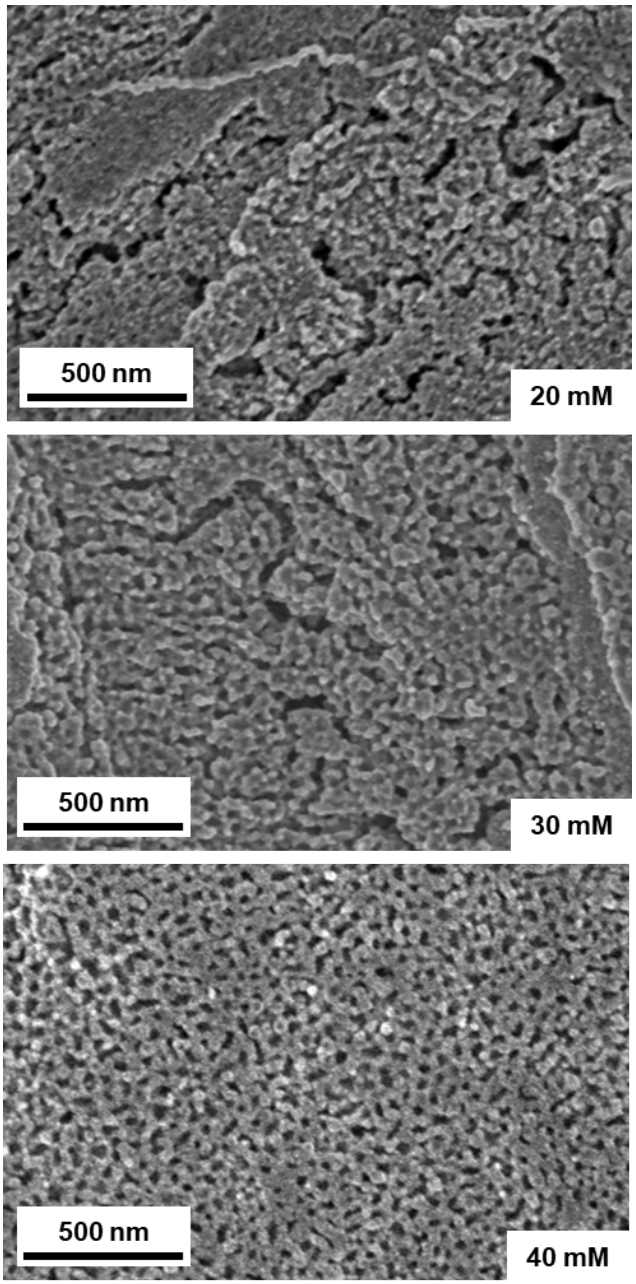

Fig. S3: SEM images of Mp-Au/Cu obtained using precursor solutions containing 20, 30, and 40 mM $HAuCl_4$ during electroless displacement deposition, showing the effect of precursor concentration on pore uniformity and film continuity.

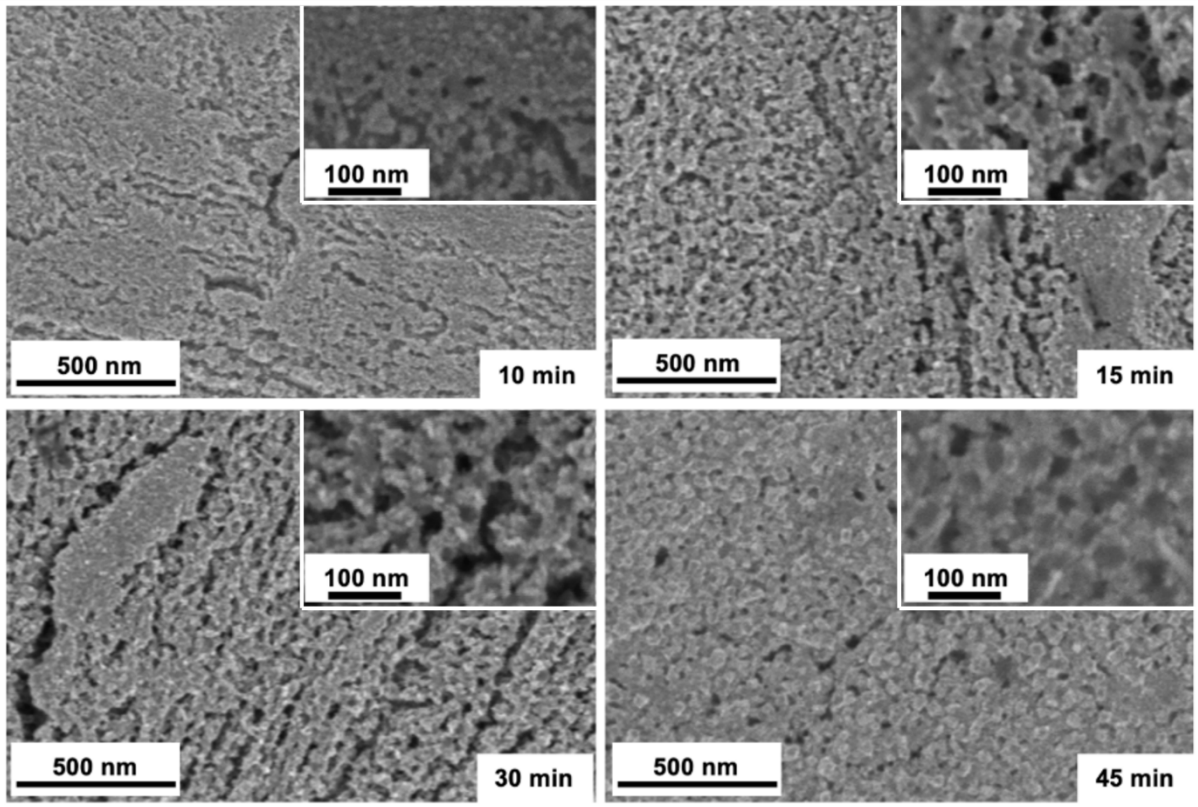

Fig. S4: SEM images of Mp-Au/Cu obtained after 10, 15, 30, and 45 min of displacement deposition, showing the progressive development of porosity and surface coverage with increasing reaction time.

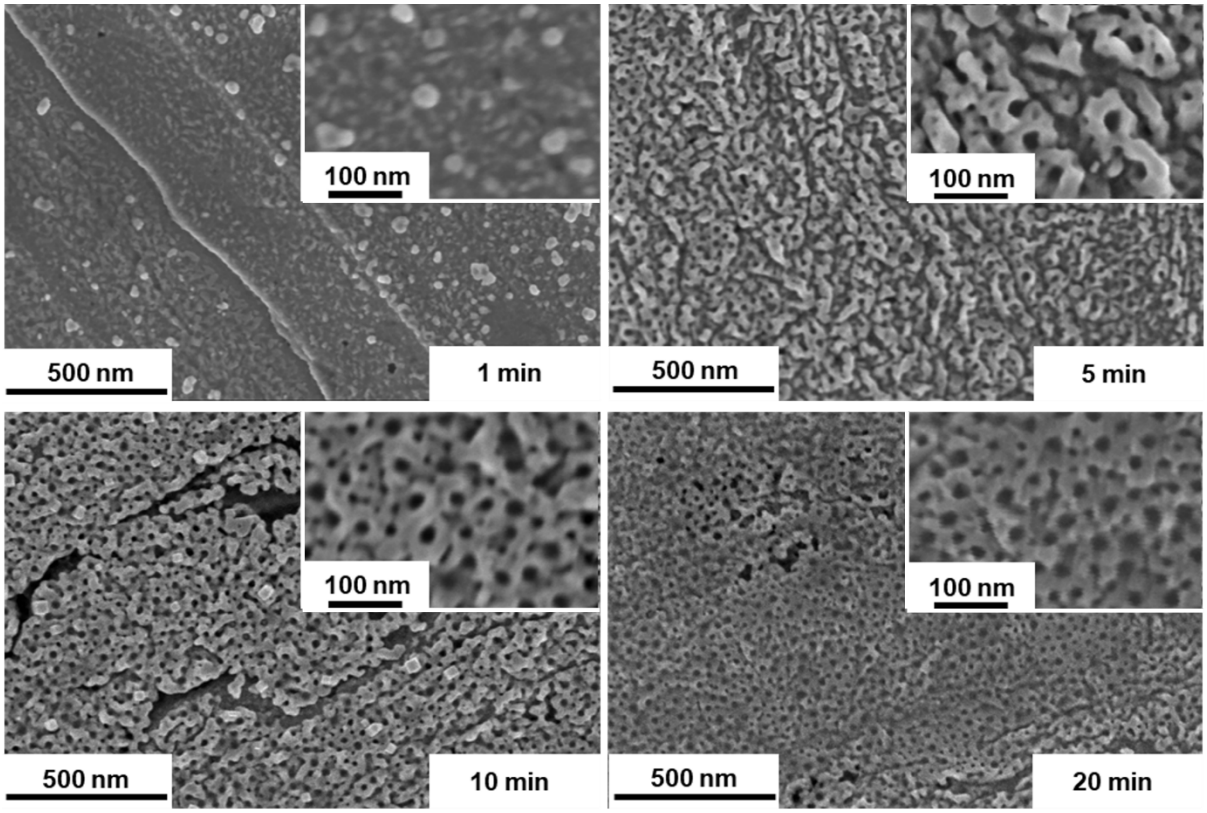

Fig. S5: SEM images of Mp-Ag/Cu obtained after 1, 5, 10, and 20 min of displacement deposition (inset: low magnification images), showing the progressive development of porosity and surface coverage with increasing reaction time.

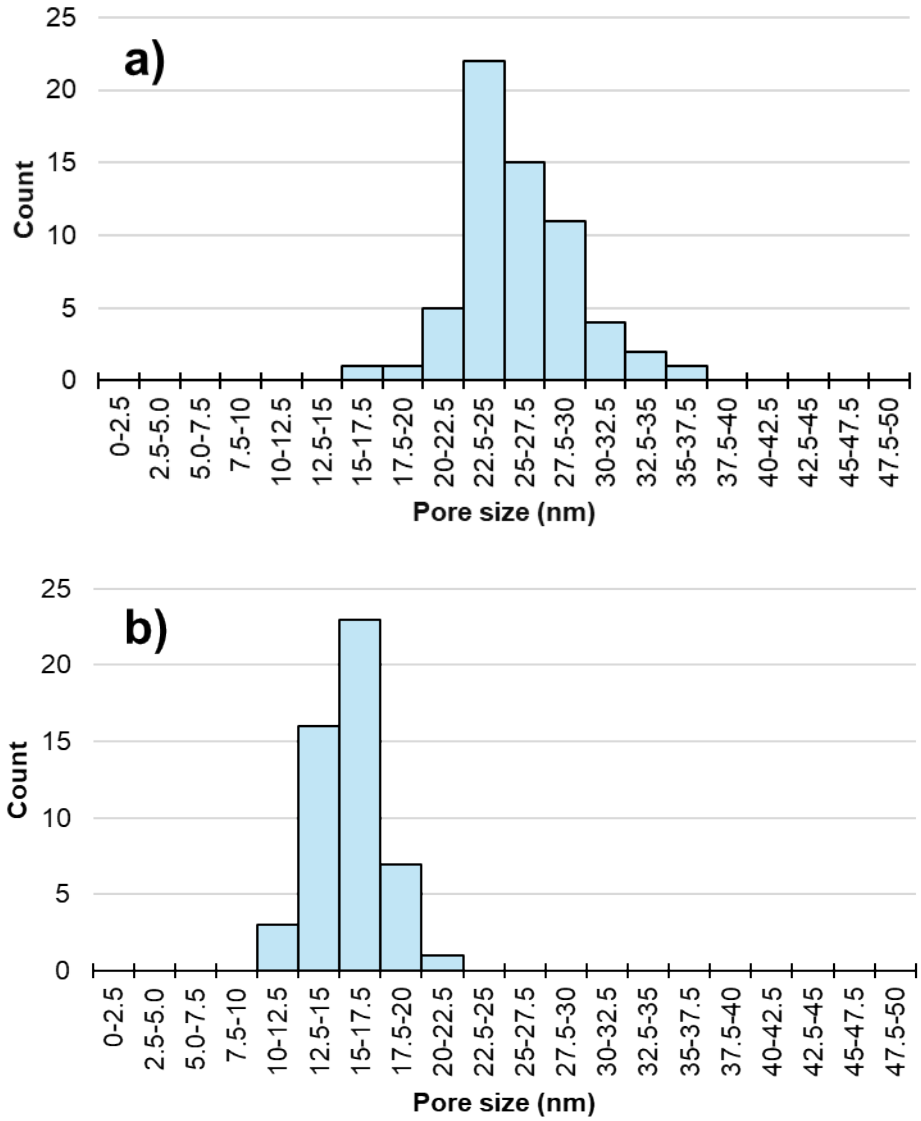

Fig. S6: Pore size distribution of (a) Mp-Au/Cu after 60 min and (b) Mp-Ag/Cu after 10 min of electroless displacement deposition, demonstrating uniform mesopore distribution in both systems.

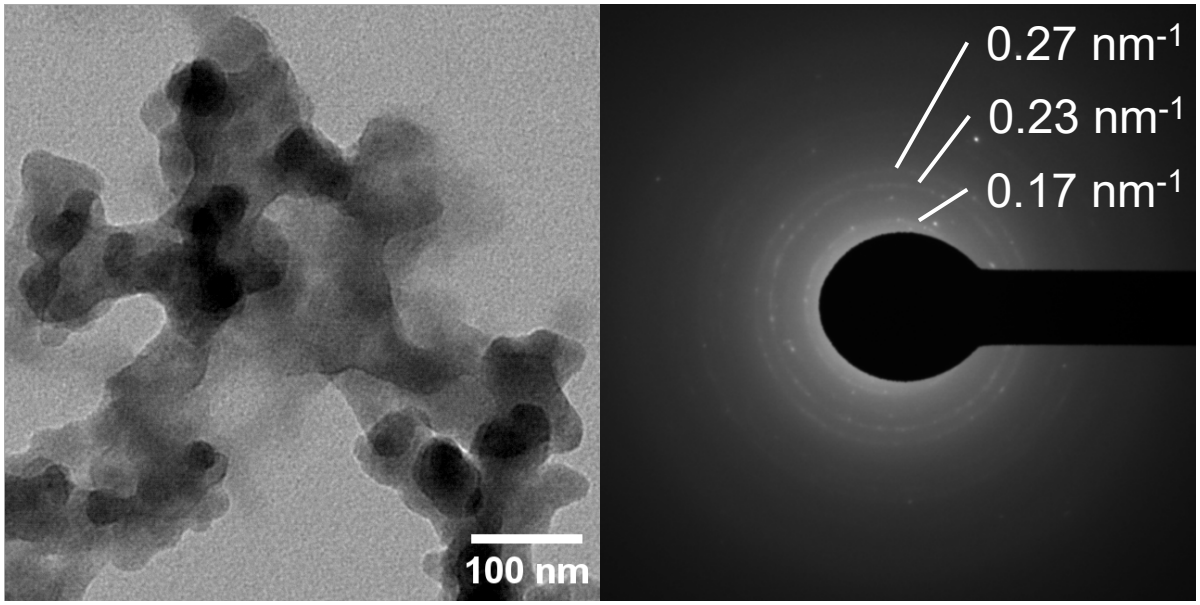

Fig. S7: TEM and SAED pattern of Mp-Au film showing diffuse rings corresponding to real-space periodicity consistent with the mesoporous architecture.

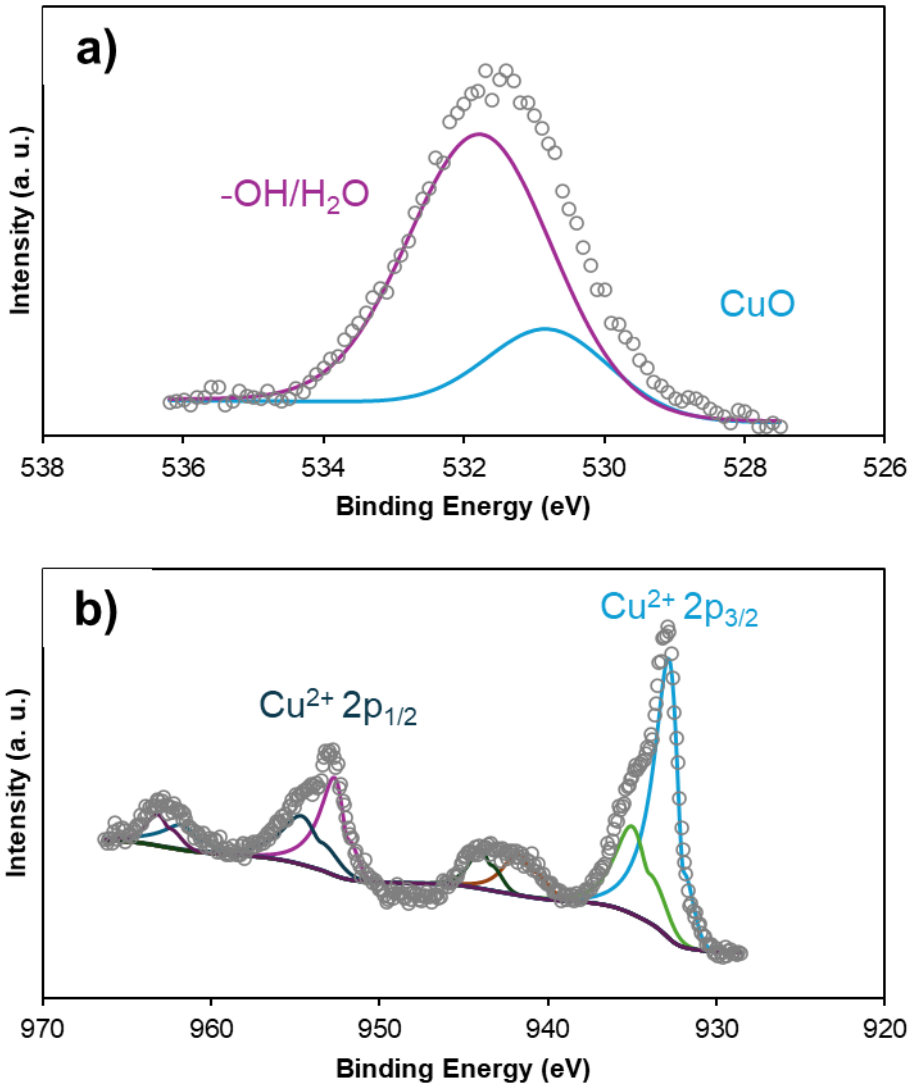

Fig. S8: High-resolution XPS spectra of Mp-Au/Cu showing characteristic (a) O1*s* and (a) Cu2*p*.

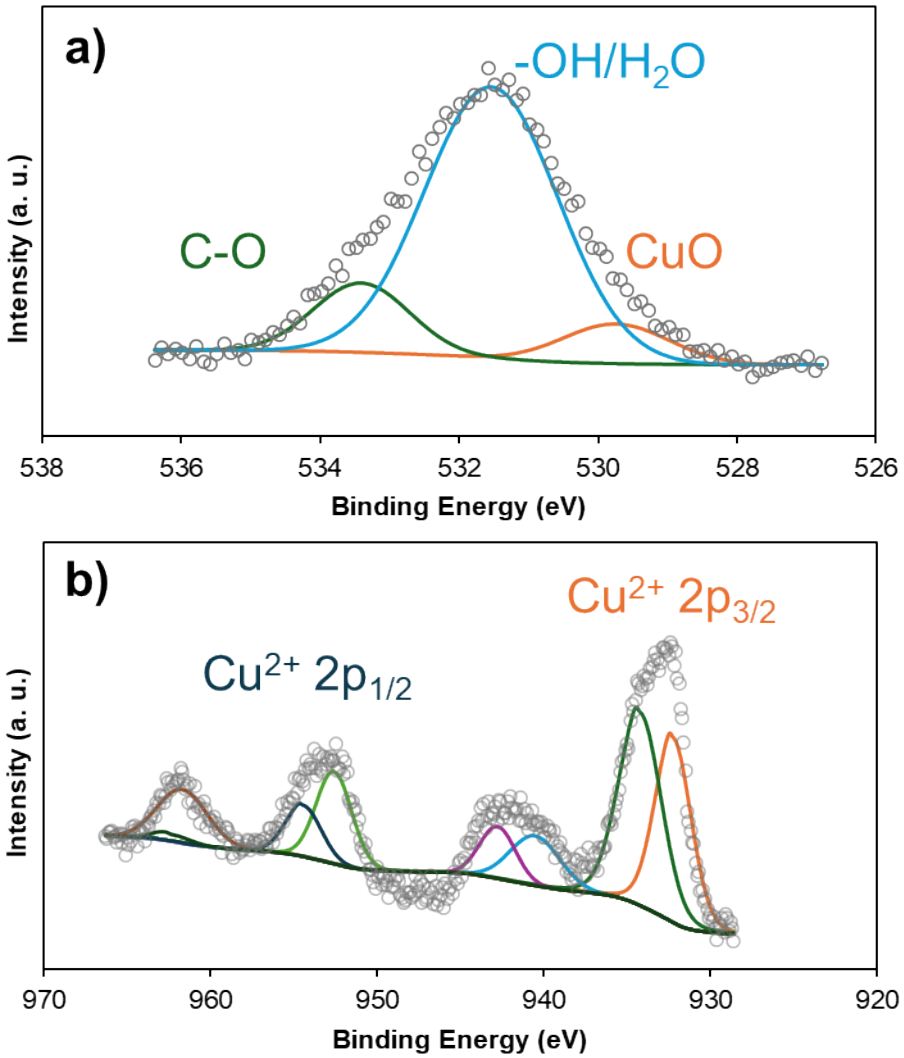

Fig. S9: High-resolution XPS spectra of Mp-Ag/Cu showing characteristic (a) O1*s* and (b) Cu2*p*.

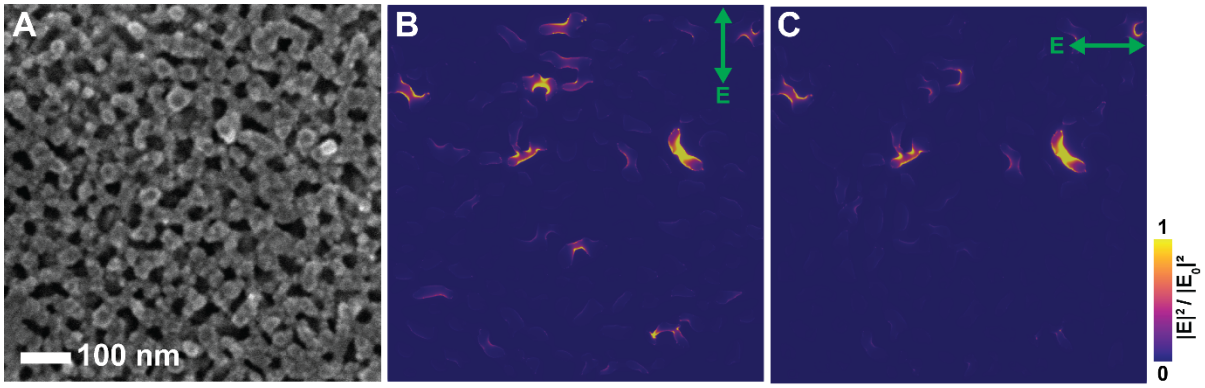

Fig. S10: SEM image of the mesoporous Au film (A). (B, C) Electric field intensity maps ($|E|^2/ |E_0|^2$) of the top surface of the film when it is excited at λ = 785 nm under plane-wave excitation with two orthogonal linear polarizations; the polarization in (C) is rotated by 90° relative to (B). Green arrows indicate the polarization direction of the incident plane wave.

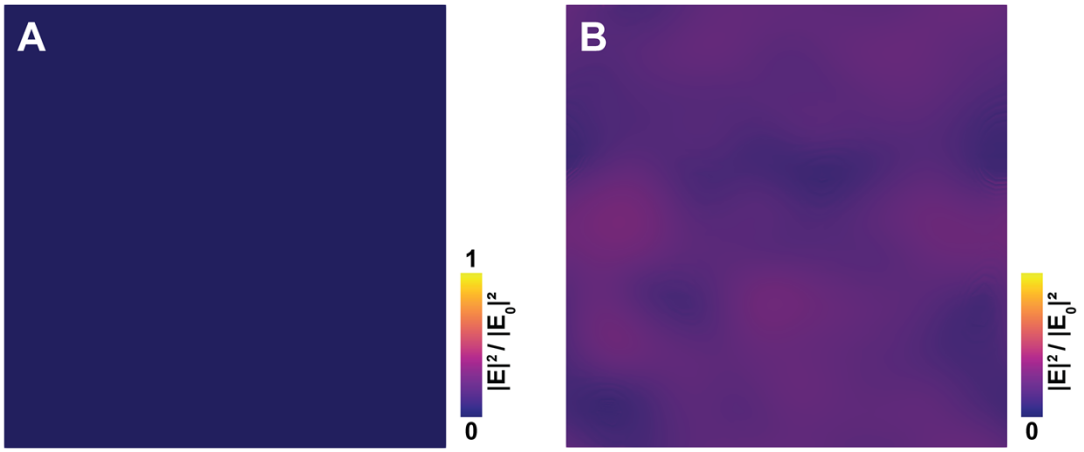

Fig. S11: Electric field intensity maps ($|E|^2/ |E_0|^2$) of the top surface of a roughened Au film with RMS = 3 nm and effective grain size = 50 nm. The field intensity in (A) is normalized to the maps of the mesoporous Au films, whereas (B) is decreased to 0.02 of the normalized field to show the disperse electric field intensity.

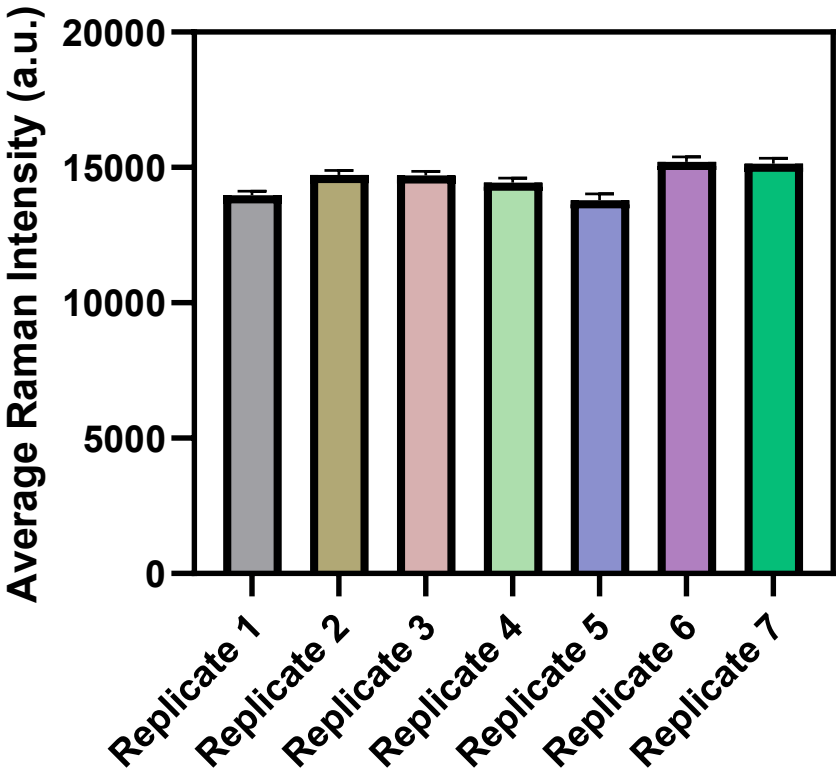

Fig. S12: Reproducibility of Mp-Au–based biosensing. Average Raman intensities from seven independent biological replicates prepared under identical conditions, showing minimal variation across replicates and confirming high reproducibility of the assay (mean ± SD, n = 3).

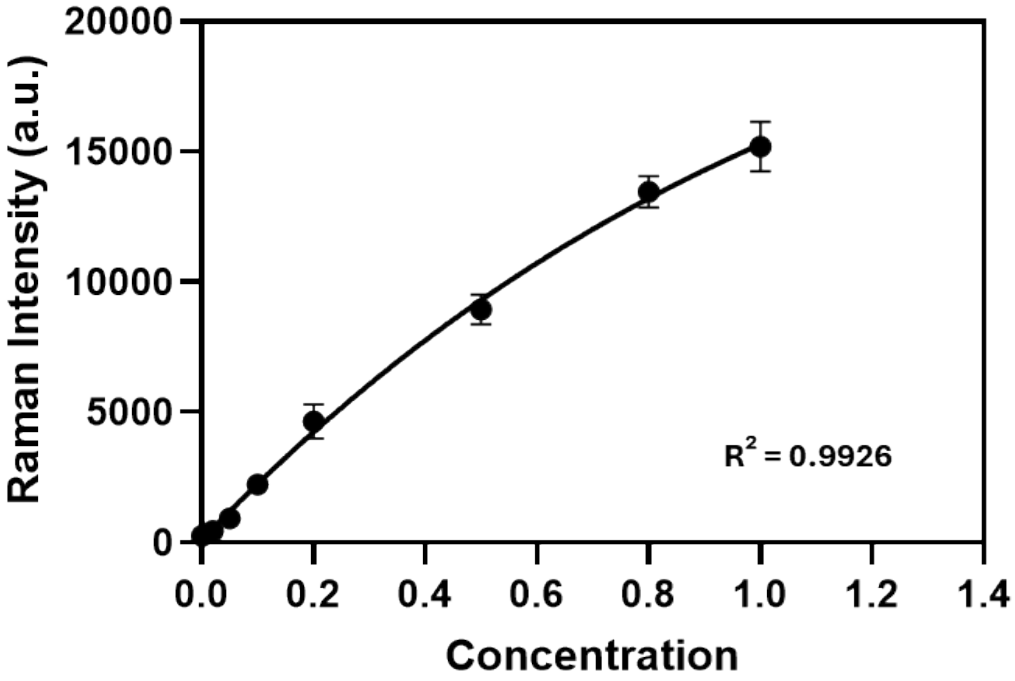

Fig. S13: A polynomial fit (3rd order) was applied to the logarithmic relationship between protein (IL-1β) concentration and SERS response, resulting in an R^2 value of 0.9926.

Supplementary Table S1: Comparison of IL-1B sensors

This table summarizes representative IL-1β biosensing platforms reported in the literature, comparing analytical formats, sample matrices, limits of detection (LOD) and linear ranges.

Platform	**Matrix**	**LOD (Linear Range)**	**Reference**
Mp-Au/Cu for SERS biosensing.	Buffer (proof-of-concept)	17.6 pg/mL (0.02-1.0 ng/mL)	This work.
AuNPs-modified fiber-optic particle plasmon resonance	Serum/biofluids	21 pg/mL (0.050-10 ng/mL)	[1]
PEDOT/4-aminothiophenol-modified SPCE Sensor.	Serum	26.25 pg/mL (1.05 ng/mL-10.5 μg/mL)	[2]
Screen-printed carbon electrode-based electrochemical dual sensor.	Serum/Saliva	0.38 pg/mL (0.5-100 pg/mL)	[3]
Electropolymerization-based molecularly imprinted electrochemical sensor.	Serum	0.23 pg/mL (0.1 pg/mL - 1.05 μg/mL)	[4]
SPR-based plastic optical fiber immunosensor.	Biofluids	271 pg/mL (0.4-70 ng/mL)	[5]
Electropolymerized MIP-based SPCE biosensor.	Serum	252 pg/mL (100-1000 pg/mL)	[6]

References

1 C. Y. Chiang, M. L. Hsieh, K. W. Huang, L. K. Chau, C. M. Chang and S. R. Lyu,

Biosens. Bioelectron., 2010, **26**, 1036–1042.

2 A. R. Cardoso, M. H. de Sá and M. G. F. Sales, *Bioelectrochemistry*, 2019, **130**, 1–9.

3 E. Sánchez-Tirado, C. Salvo, A. González-Cortés, P. Yáñez-Sedeño, F. Langa and J. M. Pingarrón, *Anal. Chim. Acta*, 2017, **959**, 66–73.

4 D. Y. Choi, J. C. Yang, S. W. Hong and J. Park, *Biosens. Bioelectron.*, 2022, **204**, 114073.

5 N. Cennamo, D. Bencivenga, M. Annunziata, F. Arcadio, E. Stampone, A. Piccirillo, F. Della Ragione, L. Zeni, L. Guida and A. Borriello, *iScience*, 2024, **27**, 108741.

6 R. Park, S. Jeon, J. W. Lee, J. Jeong, Y. W. Kwon, S. H. Kim, J. Jang, D. W. Han and S. W. Hong, *Biosensors*, 2023, **13**, 1–26.